JOURNAL OF
ENVIRONMENTAL HYDROLOGY
The Electronic Journal of the International Association for Environmental Hydrology
On the World Wide Web at http://www.hydroweb.com
VOLUME 20 2012

VARIATION IN FRESH-WATER DISCHARGE DUE TO GEOMETRIC INFLUENCES IN THE RED RIVER ESTUARY, VIETNAM

Duc H. Nguyen[1] [1]Hanoi Water Resources University, Hanoi, Vietnam
Motohiko Umeyama[2] [2]Tokyo Metropolitan University, Tokyo, Japan
Tetsuya Shintani[2] [2]Tokyo Metropolitan University, Tokyo, Japan

Fresh-water discharge is one of the most critical factors used to evaluate estuarine environments. Most previous studies have considered this discharge within the context of a tidally-averaged quantity in space and time. In this paper, a one-dimensional salt-intrusion model is proposed to predict fresh-water discharge distribution in the geometrically-complex Red River estuary. Because of changes in shape following tidal variation, the estuary branch is divided into multi-reach segments restricted by longitudinal geometric distribution in a few tidal phases. In addition, we estimated the estuary's fresh-water discharge by prescribing several geometric parameters that vary exponentially under spring and neap tide conditions. The magnitude of fresh-water discharge obtained from the analytical solution is dependent on tidal forcing and geometric parameters, and its spatial distribution is particularly sensitive to these values at high water levels.

INTRODUCTION

Fresh water carries dissolved and particulate materials from upper streams to lower pathways, which makes a significant impact on physical, geological, chemical, and biological phenomena (Skreslet, 1986; Sklar and Browder, 1998). The discharge rate changes over time with a concomitant shift in the atmospheric circulation. Although functional role of the fresh water in estuarine environments has been scientifically reviewed and relatively well understood (e.g., Slinger et al. 1994; Longley, 1994; Kimmerrer, 2002; Azevedo et al. 2010), determination of actual fresh-water inflow into tributaries and most estuaries is not well-defined due to the inherent difficulty of field observation.

Numerous studies have been conducted to quantify fresh-water discharge in tidal estuaries. Previous research has presented the issue within the context of a tidally-averaged condition in which the rate of discharge is constant both spatially and temporally. In tide-dominated estuaries, discharge rate varies because the tidal flux into the mouth of a river stops its flow and mixes with fresh water. When river discharge is low or when tidal discharge is significant, the net transport may reverse in the upstream direction. In such a case, the fresh water is bounded near the mouth during the first half of the cycle and is released from the near-mouth region into the sea during the second half (Chao 1990; Ruijter et al. 1997). The continuous succession of the event leads to pulsed distribution of fresh-water discharge. Further predictive studies in estuary regions are complicated due to these variations.

Traditionally, an estuary's daily fresh-water discharge has been determined through in-situ measurement. The local residual flow, or fresh-water discharge, was recorded after averaging the observed data throughout a full tidal cycle. Although effective, this observation technique is also labor-intensive and expensive. Moreover, during the dry season, fresh–water discharge is too small for precise measurement of its magnitude, and it is much smaller than the measurement error under the influence of tidal flows (Savenije, 2005). Therefore, fresh-water discharge is generally observed only at the upstream stations located outside the tide-affected region. Several hydrodynamic models yield high-resolution views of temporal and spatial discharge distributions (Ulses et al. 2005; Whitney and Garvine, 2006; Liu et al. 2008). However, these models require precise hydro-meteorological, geometric, and tidal data, which are not always available in the study area. The empirical-analysis method, known as the steady-flow rating curve, is also widely used for estimating river discharge as a function of water level on the basis of significant historical data. However, it is unlikely that this method determines fresh-water discharge accurately because interpolation and extrapolation errors do not factor into calculations (Dymond and Christian, 1982; Fenton, 2001; Dottori et al. 2009; Baldassarre and Montanari, 2009).

Apart from field measurement, numerical modeling, and empirical treatment, several steady-state models have been developed to elucidate estuarine salinity problems that can be used to predict fresh-water discharge. Savenije (2005) derived a salt-intrusion solution based on simplified one-dimensional hydrodynamic equations that use appropriate salinity, topographical, and tidal parameters to estimate fresh-water discharge. This model was originally developed for a single channel that considered the cross-sectional shape in tidally-averaged conditions. On the basis of this model, Nguyen et al. (2008) and Zhang et al. (2011) proposed individual models that were modified for multi-estuary use. After examining their models for the Mekong Delta in Vietnam and the Yangtze estuary in China, they concluded that with slight modifications, Savenije's model is appropriate for calculating the mean fresh-water discharge in complex geometric estuaries.

Geometric features are important factors to be considered for mathematical modeling of estuarine hydrodynamics. Savenije's model does not address the change in channel geometry due to tidal variation; cross-sectional area, width, and depth at specific locations are fixed throughout one tidal cycle. In a geometrically-complex alluvial estuary, channel dimensions vary significantly from low to high water levels (e.g., Toffolon, 2002; Prandle, 2003; Eaton, 2007). Such an estuary exhibits a prismatic shape from the upstream region to the estuary mouth with a narrower width at low water and a wider and larger area at high water (Wright et al. 1973, Brown and Davies, 2010). Geometric changes due to tidal variation affect the balance of mixing between fresh water and sea water (e.g., Toffolon et al. 2006; Gay and O'Donnell, 2007). An estuary naturally exists in equilibrium, compensating with fresh water for intruding salt by tidal advection near the mouth of the river. The river discharge, estuary shape, and tidal amplitude are curial factors to determine the behavior and appearance of the estuary. Thus, the use of tidally-averaged values in a mathematical model may conflict with actual physical parameters.

The purpose of this study is to characterize and quantify temporal and spatial variations in fresh-water discharge, which are primarily responsible for controlling salt intrusion. The methodology proposed in this paper is a series of analytical equations originally developed by Savenije (2005). We have modified the original model with different geometric parameters for both high and low water levels during spring and neap tides. The study area is the Red River estuary (RRE) near the southwest region of the Gulf of Tonkin in Vietnam. The proposed solution combined with the salt-intrusion model provides a useful tool for analyzing water-flow distribution in complex estuarine systems.

STUDY SITE AND DATA

Figure 1 shows the RRE in the northern part of Vietnam. It is the largest estuary in the Red River delta (RRD), which consists of a large low-lying plain of approximately 16,600 km^2 and includes approximately 23% of the Vietnam's population. Since 1956, the Institute of Meteorology, Hydrology, and Environment (IMHE) has measured the daily discharge at upstream stations in Son Tay and Hanoi for the Red River and in Thuong Cat for the Duong River. No systematic discharge data are available from other downstream stations. The Red River receives a large volume of fresh water with a mean annual discharge of approximately 3,800 m^3/s at the Son Tay station (based on the data of 1956-2009). The maximum of monthly mean discharge is 19,000 m^3/s in the wet season (May-October), and the minimum is 1,100 m^3/s in the dry season (November-April). The tide of the Gulf of Tonkin is predominantly a diurnal type. The mean spring and neap tidal ranges are 2.8 m and 0.6 m, respectively. Owing to the influence of river flow, the period of the rising stage is shorter than that of the falling stage, e.g., they occupy 42% and 58% of one cycle, respectively (MHMC, 1996-2009).

The datasets used in this study are salinity, tidal velocity, and topography. A series of field measurements of salinity was conducted during the dry season in 2006. The measurement was carried out from January 3 to 19, 2006, including a fortnight tidal variation. Salinity was measured at two stations: 8 km and 23 km from the mouth of the RRE. This field survey was conducted under a joint project between the Tokyo Metropolitan University and the Hanoi Water Resources University. At each location, water was sampled simultaneously at three different elevations: a height of 0.5 m from the bottom, mid-depth, and a depth of 0.5 m from the water surface. The sampling interval was one hour during the flood tide and two hours during the ebb tide. In addition to these field data, the IMHE provided official dataset for salinity at the estuary mouth. The tidal

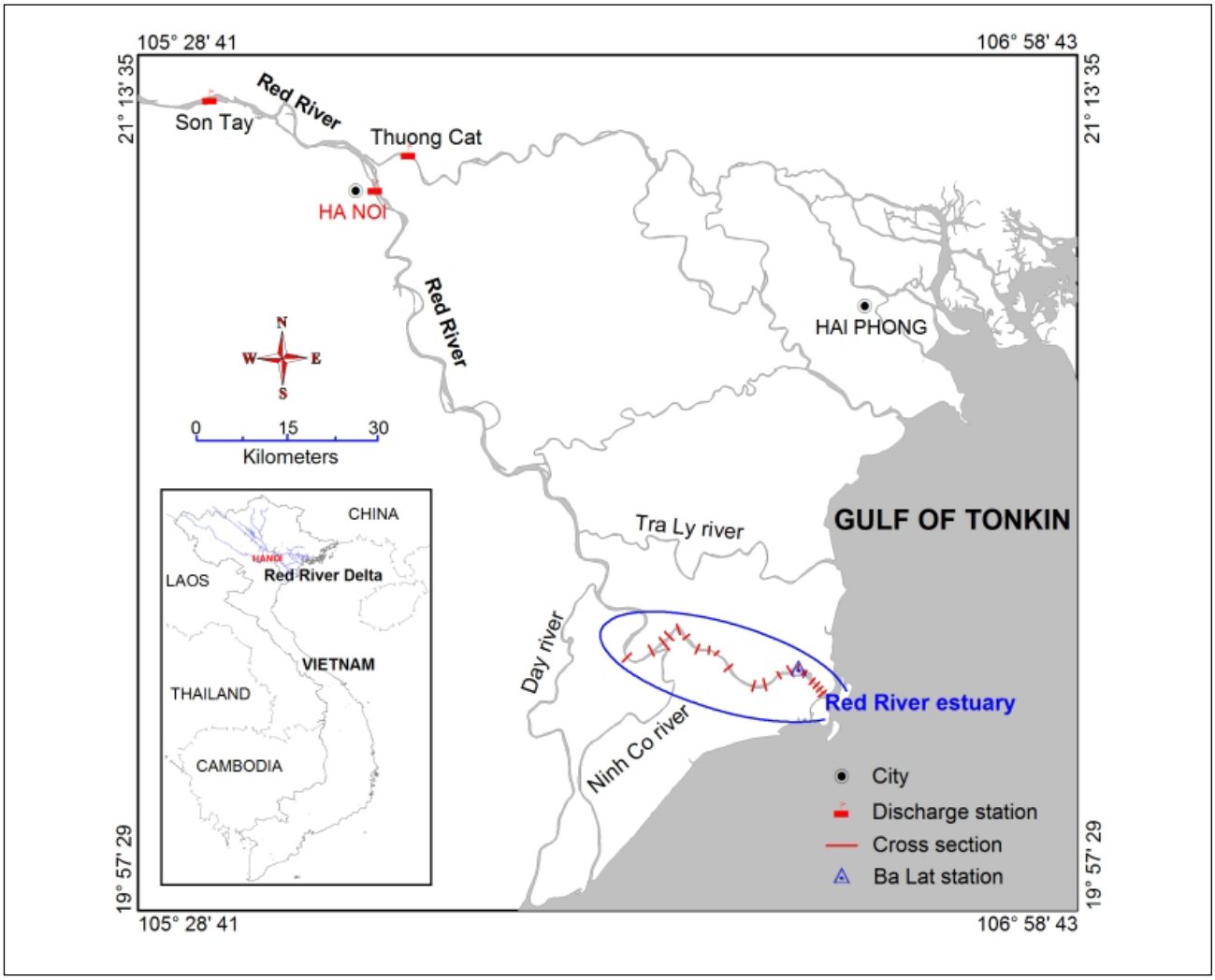

Figure 1. Map of the study area.

information was collected from the Ba Lat station, which is located near the mouth of the RRE (see in Figure 1). During the measurement period, the tidal velocity amplitude was about 0.8 m/s in spring tide and 0.3 m/s in neap tide. Detailed information on the estuarine topography was acquired by the Department of Dike Management and Flood and Storm Protection, the Ministry of Agriculture and Rural Development (MARD-DMFSP) during the dry seasons in 1999-2000 and 2007.

THEORETICAL BACKGROUND

The shape of alluvial estuaries

One may regard an alluvial estuary as an ideal channel, in which the depth is constant and the width and cross-sectional area vary exponentially in the longitudinal direction (Pillsbury, 1939; Langbein, 1963). By analyzing field data, Wright et al. (1973), Prandle (1986), and Dyer (1986) showed that the bathymetry of common estuary can be approximated by an exponential function, and later, Savenije (1993, 2005) expressed the profile as

$$N = N_0 \exp\left(\frac{-x}{l_n}\right) \tag{1}$$

where N is the geometric value at a distance from the estuary mouth (the origin), N_0 is the geometric value at the mouth, l_n is the convergence length, and x is the coordinate taken to the upstream direction from the mouth. These variables (i.e., N, N_0, and l_n) can be replaced with the parameters of A, A_0, and l_a for the cross-sectional area, B, B_0, and l_b for the width, and h, h_0, and l_d for the depth.

Salt balance equation

The longitudinal salinity distribution in a certain tidal condition can be predicted when the topography, tide, and river discharge data are available. Savenije (2005) presented an one-dimensional unsteady salt-balance equation

$$r_s A \frac{\partial S}{\partial t} + \left(Q_f + Q_t\right)\frac{\partial S(x,t)}{\partial x} - \frac{\partial}{\partial x}\left(AD(x,t)\frac{\partial S(x,t)}{\partial x}\right) = -S(x,t)R_s \tag{2}$$

where r_s is the storage width ratio between the total surface width and the actual flow width, $S(x, t)$ is the salinity, Q_f is the fresh-water discharge, Q_t is the tidal discharge, $D(x, t)$ is the longitudinal dispersion coefficient, R_s is the source term, and t is time. Because the positive x-direction points to the upstream direction, Q_f has a negative value for convenience.

Assuming no sinks and sources in the system and an equilibrium state between advective and dispersive terms at the tidally averaged (TA) condition (i.e., $\partial S/\partial t = 0$ and $Q_t = 0$), Equation (2) becomes

$$Q_f \frac{\partial S^{TA}}{\partial x} = \frac{\partial}{\partial x}\left(AD^{TA}\frac{\partial S^{TA}}{\partial x}\right) \tag{3}$$

In this formulation, the fresh-water discharge is assumed to be constant over space and time, and the cross-sectional area at a certain point along the channel is kept constant throughout one tidal cycle. Thus, Equation (3) can be integrated with respect to x to give

$$S^{TA} - S_f = \frac{AD^{TA}}{Q_f}\frac{\partial S^{TA}}{\partial x} \tag{4}$$

where S_f is the river-water salinity at the upstream end. Aside from the TA condition, the present assumption can be valid for two other extreme cases at high-water slack (HWS) and low-water slack (LWS) (Eaton, 2007). For both cases, Equation (4) has been applied to predict the longitudinal salinity distributions in several alluvial estuaries. The salinity curves at HWS and LWS can be obtained by shifting TA salinity curve over half the tidal excursion toward the sea and upstream end (Savenije, 2005; Nguyen and Savenije, 2006). Since the tidal excursion is assumed to be independent of x, the salinity profiles at HWS, LWS, and TA have the same shape.

Salt intrusion model

Based on previous work by Van den Burgh (1972), the longitudinal dispersion coefficient in an estuary can be calculated. The relationship among the dispersion coefficient, fresh-water discharge, and cross-sectional area is given by

$$\frac{dD}{dx} = K\frac{Q_f}{A} \tag{5}$$

where K is Van den Burgh's coefficient, which determines the relative strength of tide-driven and density-driven salt transports. A simple equation is proposed here to develop a model of salt intrusion, assuming a constant value of K throughout the estuary. Substituting Equation (1) into the right hand side of Equation (5) after replacing N, N_0, and l_n with A, A_0, and l_a, respectively, and integrated along the estuary, we have an analytical equation

$$\frac{D}{D_0} = \left(1 + \frac{l_a K Q_f}{A_0 D_0}\left(\exp\left(\frac{x}{l_a}\right) - 1\right)\right) \tag{6}$$

where D_0 is the dispersion coefficient at the estuary mouth. When substituting Equation (6) into Equation (4) and integrating it with respect to x, we can obtain the salinity equations for HWS, LWS, and TA. The unified cross-sectionally averaged salt-balance equation is

$$\frac{S^i - S_f}{S_0^i - S_f} = \left(1 + \frac{l_a K Q_f}{A_0 D_0^i}\left(\exp\left(\frac{x}{l_a}\right) - 1\right)\right)^{\frac{1}{K}} \tag{7}$$

where the subscript i indicates the three different tidal conditions (i.e., HWS, LWS, and TA). This one-dimensional steady advection-diffusion model has been applied to describe the salinity variations along numerous well-mixed estuaries (Savenije, 2005) and partially-mixed estuaries (Nguyen and Savenije, 2006).

Previous researchers were confronted with various difficulties when they developed the salt intrusion model. Input values such as fresh-water discharge and dispersion coefficient were not known at all points. To overcome the chronic problems, Savenije (2005) proposed a solution by introducing a new variable as

$$\alpha_0^i = -\frac{D_0^i}{Q_f} \tag{8}$$

where α^i_0 is the mixing coefficient. Combining Equations (7) and (8), the salinity curves at HWS, LWS, and TA can be fitted to salinity data. Applying this method to many estuaries in Thailand, Indonesia, Malaysia, Mozambique, Gambia, England, the Netherlands, Portugal, and the United States, Savenije (1993, 2005) also obtained an empirical equation for D_0. This relationship was generalized and improved by Nguyen and Savenije (2006) for partially- and well-mixed estuaries. The dispersion coefficient D_0, particularly for the HWS situation, is expressed as follows

$$D_0^{HWS} = 1400 \frac{E_0}{l_b} \upsilon_0 \bar{h} N_R^{0.5} \tag{9}$$

where E_0 is the tidal excursion at the mouth, defined as the difference between the intrusion lengths at HWS and LWS, υ_0 is the tidal velocity amplitude, $\bar{h}$ is the average depth over the salt intrusion length, and N_R is the Estuarine Richardson number. Fischer (1972) introduced the Estuarine Richardson number as

$$N_R = \frac{\Delta\rho}{\rho} \frac{g \bar{h} Q_f T}{\upsilon_0^2 P_t} \tag{10}$$

where $\Delta\rho$ is the relative density of fresh water with respect to sea water, ρ is the density of fresh water, T is the tidal period, and P_t is the flood volume of saltwater entering the estuary over a tidal cycle ($P_t = A_0 E$). When the flood volume can be well approximated by the product of A_0 and E_0 (= $\upsilon_0 T/\delta$) at the estuary mouth, the dispersion coefficient becomes

$$D_0^{HWS} = 1400 \frac{\bar{h}^{3/2}}{l_b} \sqrt{\frac{\Delta\rho}{\rho} g T \frac{E_0}{A_0}} \tag{11}$$

Finally, the dispersion coefficients at TA and LWS, i.e., D_0^{TA} and D_0^{LWS}, were determined from the longitudinal dispersion curve at HWS as follows

$$D_0^{TA} = D^{HWS}_{|x=E_0/2} \exp\left(-\frac{E_0}{2l_a}\right) \tag{12}$$

$$D_0^{LWS} = D^{HWS}_{|x=E_0} \exp\left(-\frac{E_0}{l_a}\right) \tag{13}$$

where D_x^{HWS} is determined through combination of Equations (6) and (11).

To compute the salinity distribution using Equations (7) and (8), A_0, l_a, K, and a_0 must be determined in advance. The value of A_0 can be obtained from bathymetry data. The convergence length l_a can be acquired by calibration of Equation (1) against the data of cross-sectional area along the estuary. The value of K is calculated from an empirical predictive equation

$$K = 0.2 \times 10^{-3} \left(\frac{E_0}{H}\right)^{0.65} \left(\frac{E_0}{C^2}\right)^{0.39} \left(1 - \delta l_b\right)^{-2.0} \left(\frac{l_b}{l_a}\right)^{0.58} \left(\frac{E_0 l_a}{A_0}\right)^{0.14} \tag{14}$$

where H is the tidal range, C is the Chezy coefficient, and $\delta = (1/H)(\partial H/\partial x)$ is the tidal-range damping rate. Although K is determined from Equation (14), in this study the value was verified from the model calibration process with salinity data measured at HWS and LWS. A sensitivity analysis was performed by changing the value of K within a reasonable range ($0 < K < 1$). When the K value is fixed, the a_0 value can be obtained by calibrating the salt intrusion model against salinity data.

Estimation of fresh-water discharge

In the case in which the salinity distribution is known, we can estimate the fresh-water discharge by dividing the computed dispersion coefficient at the estuary mouth to the calibrated mixing coefficient. Thus, rearranging Equation (8) for the discharge rate, with respect to the HWS condition, we write

$$Q_f = -\frac{D_0^{HWS}}{\alpha_0^{HWS}} \tag{15}$$

Substituting Equation (11) into Equation (15) yields

$$Q_f = -\left(\frac{1400 \dfrac{\bar{h}^{3/2}}{l_b} \sqrt{\dfrac{\Delta\rho}{\rho} g T \dfrac{E_0}{A_0}}}{\alpha_0^{HWS}} \right)^2 \tag{16}$$

METHODS

In a geometrically-complex estuary, it is sometimes difficult to describe the geometric profiles with a single exponential function (Equation (1)). In fact, a trumpet shape appears near the estuary mouth in many alluvial estuaries. In these estuaries, two or multiple segments will be needed to describe the longitudinal shape of the channel. A sketch of a geometrically-complex estuary with a trumpet shape is presented in Figure 2, in which three different cross-sectional profiles are indicated at high water level (HWL), mean water level (MWL), and low water level (LWL).

The geometric characteristics in an estuary with multi-reach segments may be described by the following exponential function

$$N = N_{j-1} \exp\left(-\frac{x - x_{j-1}}{l_{nj}} \right) \quad (j \geq 1) \tag{17}$$

where the subscript j indicates the segment number taken from the estuary mouth, $N_{j\text{-}1}$ is the geometric value at the inflection point that is located at the junction between the j-1th segment and the j^{th} segment, and $x_{j\text{-}1}$ is the distance from the mouth to the j-1th inflection point.

Assuming that the discharge rate in each segment is constant, we propose longitudinal dispersion and salinity equations as

$$\frac{D}{D_{j-1}} = \left(1 - \frac{l_{aj} K}{A_{j-1} \alpha_{j-1}} \left(\exp\left(\frac{x - x_{j-1}}{l_{aj}} \right) - 1 \right) \right) \quad (j \geq 1) \tag{18}$$

$$\frac{S - S_f}{S_{j-1} - S_f} = \left(1 - \frac{l_{aj} K}{A_{j-1} \alpha_{j-1}} \left(\exp\left(\frac{x - x_{j-1}}{l_{aj}} \right) - 1 \right) \right)^{\frac{1}{K}} \quad (j \geq 1) \tag{19}$$

where $D_{j\text{-}1}$, $A_{j\text{-}1}$, $a_{j\text{-}1}$, and $S_{j\text{-}1}$ are the dispersion coefficient, cross-sectional area, mixing coefficient, and salinity at the j-1th junction point, respectively.

This modified salt balance equation will be adapted to the RRE, after some of the assumptions are relaxed in the theoretical development. First, because of the presence of a large intertidal area throughout the whole RRE, along with the channel shape at TA, we viewed changes in the cross-sectional area, width, and depth from a new angle, taking into account of HWS and LWS. As these two levels do not lag far behind the HWL and LWL in the same day, we use the cross sectional profiles acquired at HWL and LWL to replace those at HWS and LWS, respectively. In addition, the channel width of the RRE exhibits a small convergence length near the estuary mouth, but a

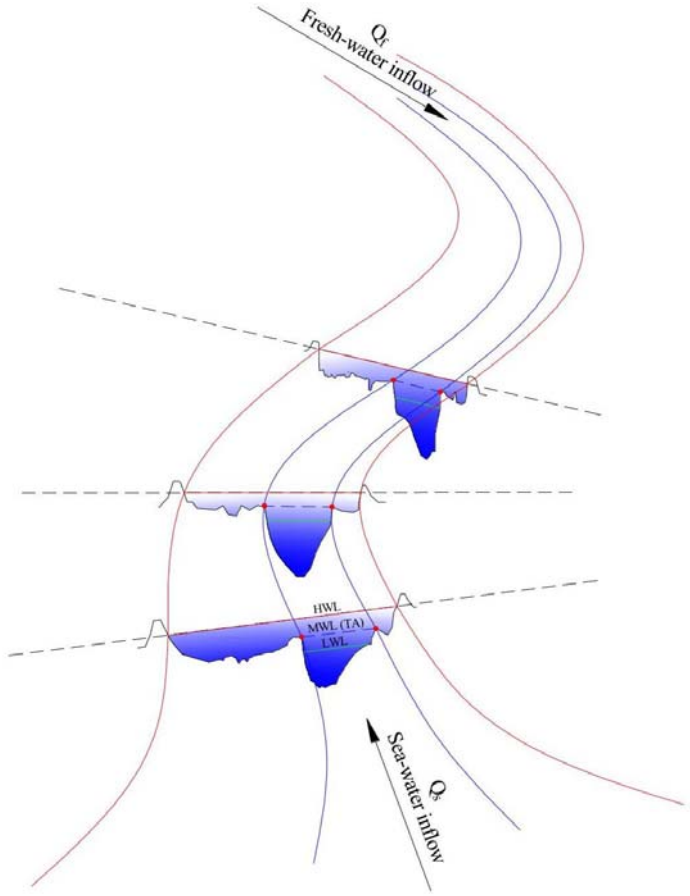

Figure 2. Sketch of a funnel-shaped estuary with complex geometry

Figure 2. Sketch of a funnel-shaped estuary with complex geometry.

large convergence length in the upstream portion. For this reason, we split the branch into two segments. Two exponential functions will be used to describe the longitudinal variation of the channel shape at each of the HWS, LWS, and TA conditions. Secondly, in contrast to the offshore salinity, the salinity at the mouth of the RRE is not constant over a tidal cycle because of the influence of river water. Three different sets of a_0 and a_1 values will be identified for the fitting of the HWS, LWS, and TA curves to the observed data with a fixed K value. Thirdly, as the salinity curves are calculated independently, values of E_0 are not estimated from the LWS and HWS curves. In the present formulation, we estimate the E_0 values based on the tidal flow data collected at the Ba Lat station. Finally, due to the variation in the geometric parameters, values of dispersion coefficient D_0 at TA and LWS will be estimated using Equation (11). In addition, for a multi-segment estuary likes the RRE, we use an average value of l_b weighted between l_{b1} and l_{b2} over the salt intrusion length (L) in the computation of D_0 (i.e. $l_b = \frac{l_{b1} \bullet x_1 + l_{b2} \bullet (L - x_1)}{L}$). Furthermore, we use the averaged depth $\overline{h}$ over the segment length instead of the mean depth at the estuary mouth (e.g., Savenije, 2005) and the averaged depth throughout the salt intrusion length (e.g., Nguyen et al. 2008). The fitted salt intrusion curve defined by Equation (19) will be used to constrain the dispersion coefficient along the RRE.

Saltwater concentrations obtained at three locations during the dry season of 2006 will be used to calibrate the salt intrusion model. The sampling schedule was designed to provide several measurements at high water and low water for each site. Because the RRE are well mixed during the dry season (IMHE, 2009), we assume that the depth-averaged salinity data represent the average value at each cross-section. After calibration of the modified model for the HWS, LWS, and TA data, values of mixing coefficient and dispersion coefficient in the downstream and upstream segments will be determined. With calibrated values of the geometric parameters, the fresh-water discharge in individual segment will be calculated for different tidal conditions using Equation (15). The results calculated at TA will be compared with the daily data obtained by a hydraulic model, both for accuracy and efficiency.

RESULTS

Topography of the RRE

Figure 3 and Table 1 present geometric characteristics along a channel in the RRE. The shapes of cross-sectional area, channel width, and depth are indicated at HWS, LWS, and TA (table only) during spring and neap tides. The cross-sectional area and width are plotted directly from bathymetric data, and the water depth represents the ratio of these two geometric values. The convergence lengths (l_{a1}, l_{a2}, l_{b1}, l_{b2}, l_{d1}, and l_{d2}) were obtained by calibrating Equation (17) against the measured data.

Computed geometric parameters in the two exponential functions fit the observed data well. The cross-sectional area, width, and depth profiles differ in profile among HWS, LWS, and TA during spring tide, but they appear identical during neap tide. It is significant to note that the neap HWS and LWS levels are nearly equal to the elevation of the estuarine floodplain, indicating that the channel width expands considerably as the tidal level exceeds the floodplain and reaches the spring HWS level. The estuary branch appears to contain an inflection point approximately 9 km from the estuary mouth. The channel displays strong convergence in the downstream segment but is weak upstream. The cross-sectional area and width expand significantly from the inflection point to the

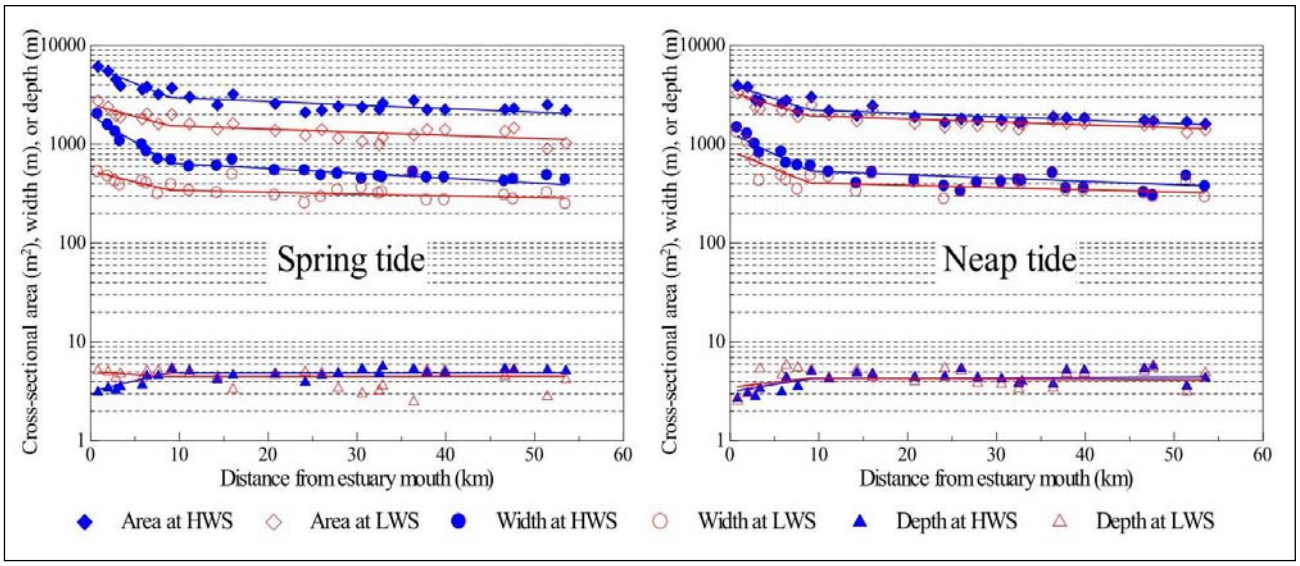

Figure 3. Cross-sectional area, width, and depth profiles of the Red River estuary (RRE). The rhombus, circle, and triangular symbols indicate the measured data. The blue curve indicates the computed result by Eq. (17) at high water slack (HWS) and the red one indicates that at low water slack (LWS).

Table 1. Geometric characteristics of the Red River estuary.

Tidal condition	A_0	B_0	h_0	A_1	B_1	h_1	l_{a0}	l_{b0}	l_{d0}	l_{a1}	l_{b1}	l_{d1}
	(m^2)	(m)	(m)	(m^2)	(m)	(m)	(km)	(km)	(km)	(km)	(km)	(km)
Spring HWS	6200	1950	2.9	2929	633	4.6	12	8	20	120	90	1000
Spring LWS	2500	530	4.9	1516	338	4.1	18	20	50	190	240	1000
Neap HWS	4000	1350	3.1	2195	549	4.2	15	10	30	140	130	1000
Neap LWS	3350	850	3.4	1909	450	4.3	16	13	40	160	190	1000
Spring/neap TA	3600	980	3.3	1980	402	4.2	15	13	40	150	150	1000

Note: A_0, B_0, and h_0 refer to the estuary mouth; A_1, B_1, and h_1 refer to the inflection location; l_{a0}, l_{b0}, and l_{d0} belong to downstream segment; and l_{a1}, l_{b1}, and l_{d1} belong to upstream segment.

mouth, particularly at HWS, while depth gradually decreases. In contrast, the area and width decrease slightly from the inflection point to the upstream, whereas the depth is nearly constant over the estuary length at a specific tidal level. The influence of tidal variation on convergence length clearly begins to emerge in these profiles; an increase in tidal level correlates with greater channel convergence.

Calibration of modified salt-intrusion model

Based on the geometric parameters, the modified salt-intrusion model was calibrated for HWS, LWS, and TA using a set of salinity data acquired at the mouth by the IMHE, and in-situ salinity data sampled at two locations during two separate spring tidal periods (January 4–8 and January 17–18, 2006) and one neap tidal period (January 11–14, 2006). The curves at HWS and LWS were fitted to maximum and minimum salinity values, respectively. The curve at TA was calibrated using salinity averaged over the measured data during a full tidal cycle. Calibrated results for model parameters (K, a_0, a_1) in the RRE are presented in Figure 4.

The computed salt-intrusion curve is in good qualitative agreement with the corresponding in-situ data. The mixing coefficients a_0 and a_1 at each tidal condition (HWS, LWS, and TA) were averaged over calibrated values, whereas the coefficient K remained constant in every tidal condition. The calibrated result of $K = 0.18$ is an acceptable value because the calculated K was 0.15. The calibrated K value is relatively small; we attribute this to the dominance of tidal mixing in the RRE. Because the K value remained constant, fitted salinity curves were sensitive to the mixing coefficients a_0 and a_1 at HWS, LWS, and TA. These mixing coefficients obtained at HWS in the downstream segment were larger than those upstream. However, the difference between these mixing coefficients at LWS and TA was insignificant. Therefore, at LWS and TA, two mixing coefficients (a_0 and a_1) can be combined into a single coefficient (a_0). This treatment corresponds to the observations of Savenije (1993, 2005), Nguyen and Savenije (2006), Eaton (2007), and Zhang et al. (2011) who used a single mixing coefficient to compute longitudinal-salinity distribution in a single-segment estuary.

The value of a_0 varied significantly with the tidal range in the downstream segment. The value obtained at HWS was generally much greater than that at LWS or TA during spring and neap tidal periods. The difference between calibrated a_0 values at HWS and LWS was 162% at spring tide and 42% at neap tide. The corresponding differences between HWS and TA were 122% at spring tide and 24% at neap tide. The value of a_1 in the upstream segment also showed a similar trend under these tidal conditions. However, these differences were unnoticed, particularly at neap tide.

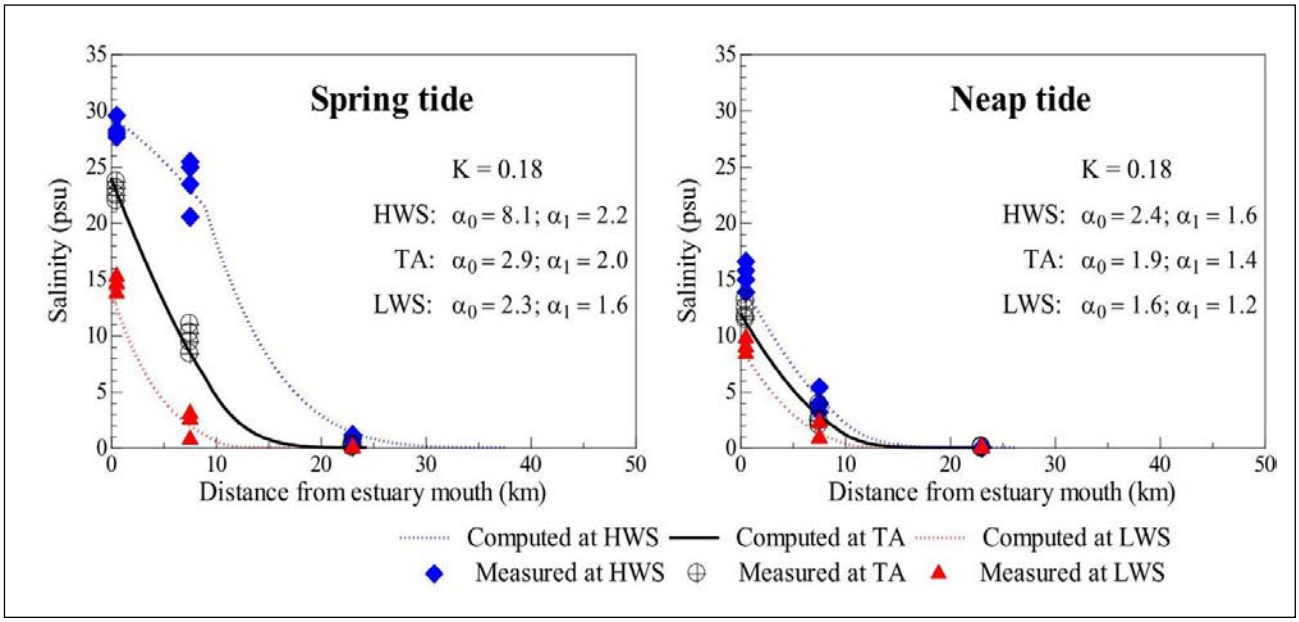

Figure 4. Salinity distributions in the RRE during spring tide and neap tide.

Salt-intrusion curves exhibit two distinct trends: a dome shape at HWS and a recession shape at LWS and TA. This difference is related to channel shape and fresh-water discharge (Savenije, 2005; Zhang et al. 2011). The dome shape occurs in a tide-dominated estuary with little fresh-water discharge and a short convergence length of the cross-sectional area near the mouth. However, the recession shape occurs in a narrow estuary, having a near-prismatic shape and significant fresh-water discharge. At HWS, the mixed water retains high salinity from the estuary mouth to the inflection point when the channel converges abruptly although salinity decreases abruptly from the inflection point to the end of the upstream segment. Under different sea-level conditions during spring and neap tides, the salt-intrusion curve remains a fixed recession shape. The salinity gradually decreases inland from its maximum value at the estuary mouth. Therefore, the Savenije's model may be applied to the RRE at LWS and TA, but it requires significant modification at HWS in a geometrically-complex estuary.

Numerical modeling of salinity distribution

Because salinity observation is limited along the estuary branch, it is difficult to validate the modified salt-intrusion model with field data under variations of geometry, discharge, and tide. In addition to the modified model, therefore, we used a hydraulic model, MIKE11, which is a professional engineering software package developed by DHI Water and Environment for simulating the flow, water quality, and sediment transport in rivers, estuaries, and other bodies of water. The advective–diffusive module of MIKE11 solves vertically integrated equations for the conservation of mass and momentum (Saint–Venant equations). The data for schematization of the hydraulic model were obtained from the IMHE and MARD-DMFSP that provide the observed discharge as an upstream boundary value, the observed tidal variation at the downstream boundary, salinity, and cross-sectional topography along the river. The model was calibrated for datasets in the dry seasons of 2000–2004 and 2006 (Vu and Bui, 2006; IMHE, 2009; Nguyen et al. 2010).

We used MIKE11 to acquire salinity distributions in the dry season of 2006 in the RRE. Figure 5 represents a comparison of salinity profiles at HWS, LWS, and TA during spring and neap tidal periods, computed by MIKE11 and the modified salt-intrusion model. The numerical prediction agrees reasonably well with the analytical result although a slight discrepancy exists between salt

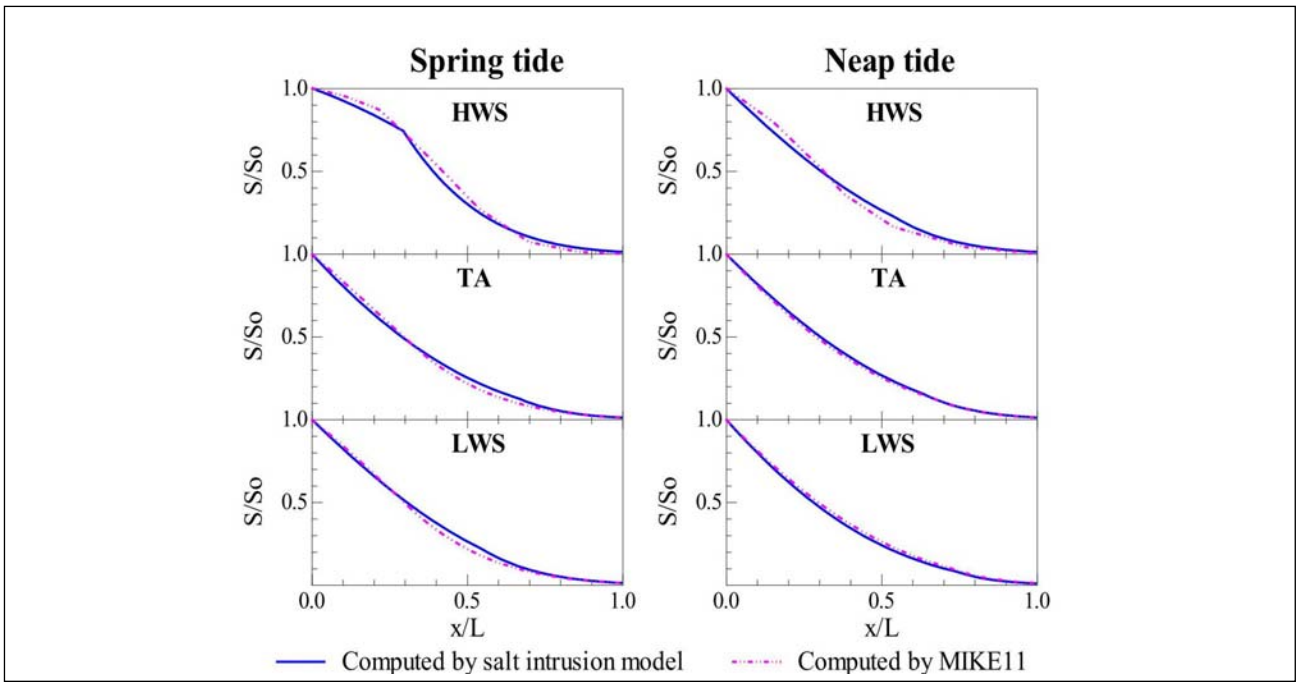

Figure 5. Comparison of computed salt intrusion curves for HWS, TA, and LWS conditions during spring and neap tides by the salt intrusion model and MIKE11.

values near the inflection point in the HWS curve. The present estimation shows a marked difference between the two curves at spring tide. Salt distribution begins as a concave shape and becomes convex within 20–40% of the salt-intrusion length. The normalized HWS curve computed by the modified salt-intrusion model does not exhibit a continuous variation, which is mainly attributed to the larger channel width and shallower depth, in addition to the sudden change in fresh-water discharge near the estuary mouth. For the other tidal cases, however, computed results by these two models appear identical without discontinuous point. Although salt intrusion along the estuary is highly sensitive to the upper and lower boundary conditions, these parameters obtained from the calibration of the modified salt-intrusion model are acceptable for common usage in the RRE.

Calculations of dispersion coefficient and fresh-water discharge

With calibrated values of the hydraulic and geometric parameters, the dispersion coefficient at the mouth was calculated for three different tidal conditions using Equation (11). Figure 6 presents the D_0 value calculated against the tidal range in the RRE. In addition, estimated values in several other global estuaries are shown (e.g., Swart et al. 1997; Lewis and Uncles, 2003; Austin, 2004; Banas et al. 2004; Savenije, 2005; Nguyen and Savenije, 2006; Shaha et al. 2011). It is significant to note that the range of D_0 is wide at spring tide but considerably narrow at neap tide. The D_0 value was 87 m^2/s at spring HWS, 871 m^2/s at spring LWS, 195 m^2/s at neap HWS, and 471 m^2/s at neap LWS, and the value varied from 393 m^2/s at neap TA to 496 m^2/s at spring TA. The present calculation result indicates that the river-mouth diffusion coefficient decreases with an increase in the tidal level. However, this result is inconsistent with the findings of Shaha et al. (2011), in which a dispersion coefficient given at a seaward end is reduced to the minimum value if the tidal force weakens. This inconsistency is attributed to specific local conditions such as geometric variation in the RRE. Due to the presence of a large intertidal area in a channel segment, the average depth at HWS is significantly smaller than that at LWS (Table 1). Because the dispersion coefficient is proportional to the three-second power of the water depth, it increases considerably

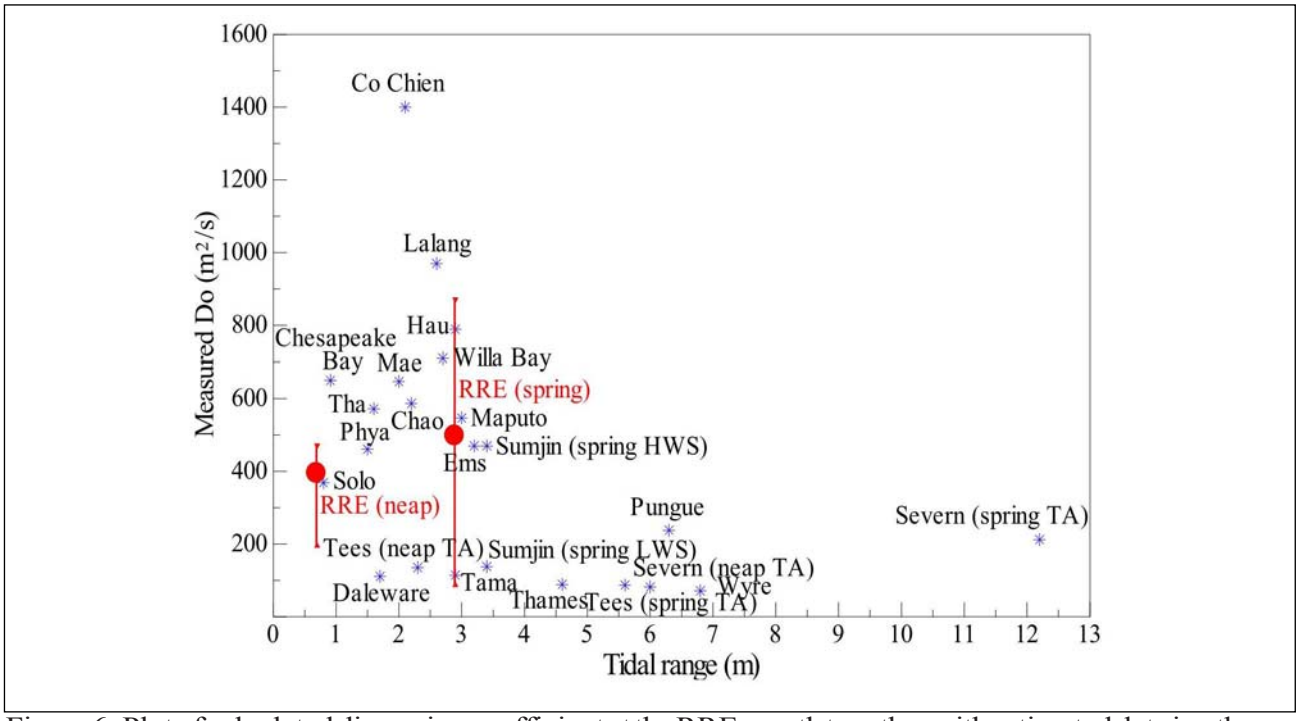

Figure 6. Plot of calculated dispersion coefficient at the RRE mouth together with estimated data in other estuaries against tidal range.

with a significant increase in depth. The dispersion coefficient D_1 at a junction can be determined from Equation (18). Among several global estuaries of various tidal ranges (0.5–4 m), the calculated dispersion coefficient is within a reasonable range.

After the calibrated values of a_0, a_1, D_0, and D_1, and geometric parameters were provided, fresh-water discharges were calculated in every segment for the various tidal conditions using Equation (16). Table 2 shows the calculated discharges for all upstream and downstream segments, in addition to daily fresh-water discharge data acquired by MIKE11. A significant difference was detected between HWS and LWS discharge and the daily value (TA). Calculated fresh-water discharge was lowest at HWS and highest at LWS due to the influence of flood–ebb modulation of tide to river flow. The computed results presented here for HWS and LWS can represent discharge rates at HWL and LWL, respectively. The difference between HWS and HWL patterns or between LWS and LWL patterns is attributed to uncertainty in the tidal stage, at which maximum and minimum salinity values were acquired.

Fresh-water discharge computed by the salt-intrusion model at spring HWS exhibited a sudden change at the intersection between upstream and downstream segments, which may possibly be due to significant changes in geometry and mixing coefficients. In contrast, under the other tidal conditions at LWS and TA, differences in fresh-water discharge computed between the downstream and upstream segments were negligible. These computed results are in agreement with previous studies that presumed a constant value of fresh-water discharge over the entire estuary length. When the computed results by the salt-intrusion model and MIKE11 are compared, discharge for the TA condition by the former model agrees reasonably well with that by the latter. This finding supports our argument of fresh-water-discharge distribution in a multi-segment estuary using the analytical model. Reconsidering the inconsistency of fresh-water inflow into an estuary, the calculation method provides an important step for the investigating fresh-water discharge at high and low tides.

Table 2. Calculation of freshwater discharge at different water levels in spring and neap tides.

Tidal condition	$\bar{h}$ (m)	l_b (km)	Q_{f0} (m^3/s)	Q_{f1} (m^3/s)	$\bar{Q}_f$ by MIKE11 (m^3/s)
Spring HWS	2.95	67.6	11	41	
Spring TA	3.44	79.4	171	167	189
Spring LWS	4.61	123.5	379	373	
Neap HWS	3.05	59.8	81	97	
Neap TA	3.44	60.0	207	196	199
Neap LWS	3.51	63.6	295	307	

DISCUSSION

In this study, we improved a salt-intrusion model to estimate fresh-water discharge in a geometrically-complex estuarine system. Although the previous model has the ability to investigate the distribution of fresh-water discharge rates at high and low tides, limitations remain in the application to actual complex estuaries. The present method will be useful for estimating the hydrologic quantities of estuaries when adequate observation points are unavailable.

The geometric feature is the most important factor because it influences salt-intrusion length and river water velocity. A precisely increased description in the geometric complexity may yield a more reliable result. Therefore, geometric parameters were distinguished among HWS, LWS, and TA in order to avoid errors. However, the high sediment amount in the RRE causes the river mouth to continually spread seaward (Van Maren and Hoekstra, 2004), which should be considered by additional bathymetry observations.

Computation of fresh-water discharge is sensitive to a number of parameters in the salt-intrusion model such as K, a_0, a_1, E_0, and D_0. The K value was acquired from the calibration process with salinity data obtained in 2006. Although the calibrated value is fairly consistent with the predictive data, Van den Burgh's equation for K is can be re-evaluated after collecting detailed observation data such as tidal excursion, tidal velocity, and tidal damping rate. Because the K value remained constant throughout this analysis, the model was sensitive only to the mixing coefficients a_0 and a_1. Fresh-water discharge alters a degree of salt intrusion primarily through these mixing coefficients, which depend on topographical data. With an increase in the cross-sectional area from low to high water levels, these mixing coefficients increase in conjunction with a smaller convergence length. Hence, analyzing variation in geometric characteristics under different tidal conditions can help explain changes in model coefficients and provide some clarifications for the effect of different aspects on the fresh-water discharge. If a complex, multi-segment estuary is analyzed, additional salinity data must be collected in order to calibrate the model. Because observation was performed only at three sampling locations in this study, the calibrated results may be less reliable. Further investigation based on a more sufficient dataset for salinity is required for a considerable improvement of the present study.

The tidal excursion E_0 and dispersion coefficient D_0 are difficult to determine properly in reality. In the original model, E_0 is estimated based on the fitted HWS and LWS salinity curves. Because these salinity curves were acquired independently, E_0 was determined based on the measured tidal currents. The coefficient D_0 is a critical parameter when Equations (15) and (16) are used for determining the fresh-water-discharge rate. For each tidal condition, the D_0 value was estimated by Equation (11) and was inversely proportional to the tidal level. Linden and Simpson (1988) considered that turbulence generated by strong tidal currents effectively reduce the dispersing action of velocity shear; consequently, the D_0 value tends to decrease as the tidal level

increases. Without corresponding velocity data, estimating the relative contribution of the shear dispersion by tidal currents becomes impossible. The present results demonstrated that the dispersion coefficient increases with fresh-water discharge. This finding is consistent with previous studies (e.g., Lewis and Uncle 2003; Shaha et al. 2011).

Demonstrating fresh-water distribution in a multi-segment estuary is slightly complicated because of the variation in bathymetric parameters defining the estuary shape in addition to the tidal change. The pronounced influence by geometric parameters is evident in the magnitude of fresh-water discharge shown in Table 2. Extension of RRE floodplain creates a significantly wider and shallower channel toward the coastal delta. A shorter convergence length results in a lower discharge rate at high water levels. In contrast, the channel becomes deeper and narrower with a greater convergence length at low water levels. As expected, fresh-water discharge value was high in this case.

During spring tide, river water flow is obstructed in the RRE because of significant sea-water advection from the Gulf of Tonkin. During ebb tide, river water drains, thereby expelling the sea water from the mouth. This sequential phase modulation of water discharge is consistent with the investigation in the Rhine estuary by Van Alphen et al. (1988), who used hydrographic data to illustrate that nontransported river water exhibits a pinching-off effect in reversed tidal conditions. Ruijter et al. (1997) gave a principle criterion that concerns the pulsed distribution of fresh-water discharge over one tidal cycle: the river discharge is halted if the value of tidal current is larger than that of river velocity. According to the measured current profiles within the RRE in the dry season of 2000 by Van Maren and Hoekstra (2004), the maximum outflow and inflow were 0.49 m/s and -0.29 m/s, respectively, during spring tide, and 0.24 m/s and -0.06 m/s, respectively, during neap tide. These values imply that the average tidal current and river flow were 0.39 m/s and 0.10 m/s, respectively, for the former and 0.15 m/s and 0.09 m/s, respectively, for the latter. These velocity changes may indicate a spring–neap variation with a pulsed fresh-water discharge if they comply with the criterion of Ruijter et al. (1997). This finding from the observation agrees well with our calculated results (Table 2).

It is significant to note that the calculated fresh-water discharge was spatially varied at HWS but was nearly constant over the estuary length at LWS and TA. This geometric variation plays a crucial role in mixing rate and tidal forcing during each tidal phase. The present finding is consistent with that of Horrevoets et al. (2004), who illustrated the influence of fresh-water flow on spatial variations of both mixing and tidal-damping rates in the Schelde estuary. This type of data is particularly significant in shallow estuaries, in which tidal flux dominates saline transport. In computations, fresh-water discharge was maintained constant throughout each segment length; thus, the discharge became discontinuous at the inflection point. To overcome this discrepancy, a sufficient number of segments with detailed salinity measurements must be provided. Unfortunately, the salinity data lack a critical value to support the proposed mechanism of discharge along the RRE. Although several three-dimensional numerical models support the calculation of fresh-water discharge spatially, their application is beyond the scope of the present study.

CONCLUSIONS

We used a salt-intrusion model to estimate temporal and spatial variations of fresh-water discharge in the RRE. Owing to changes in the estuary shape and size following tidal variations, we split the estuary into two segments, taking into account of two exponentially shaped scales for

geometric characteristics under HWS, LWS, and TA conditions. Model parameters were calibrated using bathymetry and salinity data measured along the RRE during spring and neap tides. The present method allowed us to estimate fresh-water distribution for multiple segments on the basis of the modified one-dimensional, steady-state salt-intrusion model. We found that geometric feature is one of the most important factors affecting the character of salt intrusion curves and the temporal and spatial distributions of fresh-water discharge. A comparison of analytical and numerical salt variations in several tidal conditions showed reasonable agreement although there is a small discrepancy near the inflection point at HWS. Overall, the analytical model provided an acceptable estimation of the distributions of the fresh-water discharge. This study will serve as a useful guide for future research of water resources in tidal rivers and estuaries.

ACKNOWLEDGMENTS

The authors would like to acknowledge the Tokyo Metropolitan Government for financial support from the Asian Human Resources Fund under the project "Solutions for the water related problems in Asian metropolitan areas." We also would like to thank Associate Professor Dr. Tran Ngoc Anh (Faculty of Hydrology, Meteorology, and Oceanography, Vietnam National University), Dr. Zhang Jingjie (Singapore Delft Water Alliance, National University of Singapore), and Dr. Nghiem Tien Lam (Dynamic Solutions-International, LLC) for their helpful comments and suggestions to improve this work.

REFERENCES

Austin, J.A. 2004. Estimation of effective longitudinal dispersion in the Chesapeake Bay. Estuarine, Coastal and Shelf Science, Vol. 60, pp. 359-368.

Azevedo, I.C.,A.A. Bordalo, and P.M. Duarte. 2010. Influence of river discharge patterns on the hydrodynamics and potential contaminant dispersion in the Douro estuary. Water Research, Vol. 44, pp. 3133-3146.

Baldassarre, D.G., andA. Montanari. 2009. Uncertainty in river discharge observations: a quantitative analysis. Hydrology and Earth System Science, Vol. 13, pp. 913-921.

Banas, N.S., B.M. Hickey, P. MacCready, and J.A. Newton. 2004. Dynamics of Willapa Bay, Washington, a highly unsteady partially mixed estuary. Journal of Physical Oceanography, Vol. 34, pp. 2413-2427.

Brown, J.M., and A.G. Davies. 2010. Flood/ebb tidal asymmetry in a shallow sandy estuary and the impact on net sand transport. Journal of Geomorphology, Vol. 114, pp. 431-439.

Chao, S.Y. 1990. Tidal modulation of estuarine plumes. Journal of Physical Oceanography, Vol. 20, pp. 1115-1123.

Dottori, F., M.L.V. Martina, and E. Todini. 2009. A dynamic rating curve approach to indirect discharge measurement. Hydrology and Earth System Science, Vol. 13, pp. 847-863.

Dyer, K.R. 1986. Coastal and Estuarine Sediment Dynamics. John Wiley & Sons, 342 p.

Dymond, J.R., and R. Christian. 1982. Accuracy of discharge determined from a rating curve. Hydrological Sciences Journal, Vol. 27(4), pp. 493-504.

Eaton, T.T. 2007. Analytical estimates of hydraulic parameters for urbanized estuary - Flusing Bay. Journal of Hydrology, Vol. 347, pp. 188-196.

Fenton, J.D. 2001. Rating Curves: Part 1-Correction for Surface Slope. Proc. Conference on Hydraulics in Civil Engineering, Hobart,Australia, pp. 309-317.

Fischer, H.B. 1972. Mass transport mechanisms in partially mixed estuaries. Journal of Fluid Mechanics, Vol. 53(4), pp. 671-687.

Gay, P.S., and J. O'Donnell. 2007.A simple advection-dispersion model for the salt distribution in linearly tapered estuaries. Journal of Geophysical Research, Vol. 112, C07021.

Horrevoets,A.C., H.H.G. Savenije, J.N. Schuurman, and S. Graas. 2004.The influence of river discharge on tidal damping in alluvial estuaries. Journal of Hydrology, Vol. 294, pp. 213-228.

IMHE. 2009. Forecasting of tidal propagation and salinity intrusion in the Red River Delta.Technical report, 183 p (in Vietnamese).

Kimmerer, W.J. 2002. Physical, biological, and management responses to variable freshwater flow into the San Francisco estuary. Estuaries, Vol. 25(6B), pp. 1275-1290.

Langbein, W.B. 1963. The hydraulic geometry of a shallow estuary. Bulletin of International Association of Scientific Hydrology, Vol. 8, pp. 84-94.

Lewis, R.E., and R.J. Uncles. 2003. Factors affecting longitudinal dispersion in estuaries of different scale. Ocean Dynamics, Vol. 53, pp. 197-207.

Linden, P.F., and J.E. Simpson. 1988. Modulated mixing and frontgenesis in shallow seas and estuaries. Continental Shelf Research, Vol. 8, pp. 1107-1127.

Liu, W.C., W.B. Chen, R.T. Cheng, and M.H. Hsu. 2008. Modelling the impact of wind stress and river discharge on Danshuei River plume. Applied Mathematical Modelling, Vol. 32, pp. 1255-1280.

Longley, W.L. 1994. Freshwater inflows to Texas bays and estuaries: Ecological relationships and methods for determination of needs. Texas Water Development Board, Austin, Texas.

MHMC, Marine Hydro-meteorological Center, Hanoi, Vietnam. 1996-2009. Annual tide tables.

Nguyen, A.D., and H.H.G. Savenije. 2006. Salt intrusion in multi-channel estuaries: a case study in the Mekong Delta, Vietnam. Hydrology and Earth System Science, Vol. 10, pp. 743-754.

Nguyen, A.D., H.H.G. Savenije, D.N. Pham, and T.T. Tang. 2008. Using salt intrusion measurements to determine the freshwater discharge distribution over the branches of a multi-channel estuary: The Mekong Delta case. Estuarine, Coastal and Shelf Science, Vol. 77, pp. 433-445.

Nguyen, H.D,T. Shintani, and M. Umeyama. 2011. Influence of saline intrusion during the dry season in Red river and Thai Binh river systems, Vietnam. ISEH Conference Proceeding, Athens, Greece, pp. 317-327.

Prandle, D. 1986. Generalized theory of estuarine dynamics. In: Physics of shallow estuaries and bays. V.D. Kreeke & J. Ed. Berlin: Springer-Verlag, Lecture Notes on Coastal and Estuarine Studies, No. 16, pp. 42-57.

Prandle, D. 2003. Relationships between tidal dynamics and bathymetry in strongly convergent Estuaries. Journal of physical oceanography, Vol. 33, pp. 2738-2750.

Pillsbury, G. 1939. Tidal Hydraulics. US Corps of Engineers, Vicksburg, USA.

Ralston., D.K., W.R. Geyer, and J.A. Lerczak. 2008. Subtidal salinity and velocity in the Hudson River estuary: Observations and modeling. Journal of Physical Oceanography, Vol. 38, pp. 753-770.

Ruijter, W.P.M.D., A.W. Visser, and W.G. Bos. 1997.The Rhine outflow: A prototypical pulsed discharge plume in a high energy shallow sea. Journal of Marine Systems, Vol. 12, pp. 263-276.

Savenije, H.H.G. 1993. Predictive model for salt intrusion in estuaries. Journal of Hydrology, Vol. 148(1-4), pp. 203-218.

Savenije, H.H.G. 2005. Salinity and Tides in Alluvial Estuaries. Elsevier, Amsterdam, 197 p.

Shaha, D.C., Y.K. Cho, M.T. Kwak, S.R. Kundu, and K.T. Jung. 2011. Spatial variation of the longitudinal dispersion coefficient in an estuary. Hydrology and Earth System Science, Vol. 15, pp. 3679-3688.

Sklar, F.H., and J.A. Browder. 1998. Coastal environmental impacts brought about by alterations to freshwater flow in the Gulf of Mexico. Environmental Management, Vol. 22, pp. 547-562.

Skreslet, S. 1986.The Role of Freshwater Outflow in Coastal Marine Ecosystems. NATO ASI Series, G edition. SpringerVerlag, Berlin, Germany.

Slinger, J.H., S. Taljaard, and J.L. Largier. 1994. Changes in estuarine water quality in response to a freshwater flow event. In: Changes in Fluxes in Estuaries. Implications from Science to Management. (ed) K.R. Dyer & R.J. Orth, pp. 51-56.

Swart, H.E.D., V.N.D. Jonge, and M. Vosbeek. 1997. Application of the tidal random walk model to calculate

water dispersion coefficients in the Ems estuary. Estuarine, Coastal and Shelf Science, Vol. 45, pp. 123-133.

Toffolon, M. 2002. Macro-scale morphological characterisation of the western Scheldt. Technical report, Delft Cluster Report, 71 p.

Toffolon, M., G. Vignoli, and M. Tubino. 2006. Relevant parameters and finite amplitude effects in estuarine hydrodynamics. Journal of Geophysical Research, Vol. 111, C1OO14.

Uncles, R.J., R.C.A. Elliott, and S.A. Weston. 1985. Observed fluxes of water, salt and suspended sediment in a partially mixed estuary. Estuarine, Coastal and Shelf Science, Vol. 20, pp. 147-167.

Ulses, C., C. Grenz, P. Marsaleix, E. Schaaff, C. Estournel, S. Meule, and C. Pinazo. 2005. Circulation in a semi-enclosed bay under influence of strong freshwater input. Journal of Marine Systems, Vol. 56, pp. 113-132.

Van Alphen, J.S.L.J., W.P.M.D. Ruijter, and J.C. Borst. 1988. Outflow and three dimensional spreading of Rhine river water in the Netherlands coastal zone. In: Dronkers. I., Van Leussen, W. (Eds.), Physical Processes in Estuaries. Springer, Berlin, pp. 70-92.

Van den Burgh, P. 1972. Ontwikkeling van een methode voor het voorspellen van zoutverdelingen in estuaria, kanalen en zeeen. Rijkwaterstaat Rapport.

Van Maren, D.S., and P. Hoekstra. 2004. Seasonal variation of hydrodynamics and sediment dynamics in a shallow subtropical estuary: the Ba Lat River, Vietnam. Estuarine, Coastal and Shelf Science, Vol. 60, pp. 529-540.

Vu, M.C, and D.D. Bui. 2006. Assessment of saline water intrusion into estuaries of Red-Thai Binh River during dry season having considered water released from upper reservoirs and tidal fluctuation. Proceeding of the Vietnam-Japan Estuary Workshop, Hanoi, Vietnam.

Whitney, M.M., and R.W. Garvine. 2006. Simulating the Delaware Bay buoyant outflow: Comparison with observations. Journal of Physical Oceanography, Vol. 36, pp. 3-21.

Wright, L.D., J.M. Coleman, and B.G. Thom. 1973. Process of channel development in a high tide range environment: Cambridge Gulf-Ord river delta, Western Australia. Journal of Geology, Vol. 81, pp. 15-41.

Zhang, E., H.H.G. Savenije, H. Wu, Y. Kong, and J. Zhu. 2011. Analytical solution for salt intrusion in the Yangtze Estuary, China. Estuarine, Coastal and Shelf Science, Vol. 91, pp. 492-501

ADDRESS FOR CORRESPONDENCE
Duc H. Nguyen
Department of River Engineering and Natural Disaster Management
Hanoi Water Resources University
No. 75 Tay Son street, Dong Da district
Hanoi, Vietnam

Email: ducnh@wru.edu.vn